# Title: Cannabinoid Combination Targets *NOTCH1*-Mutated T-ALL Through the Integrated Stress Response Pathway


## Authors

Elazar Besser[1], Anat Gelfand[1], Shiri Procaccia[1], Paula Berman[1], David Meiri[1, *]

## Affiliations

[1] The Laboratory of Cancer Biology and Cannabinoid Research, Faculty of Biology, Technion-Israel Institute of Technology, Haifa 3200003, Israel

* Corresponding author: David Meiri, The Laboratory of Cancer Biology and Cannabinoid Research, Faculty of Biology, Technion- Israel Institute of Technology, Haifa 3200003, Israel; Phone: +972-77-8871681; Fax: +972-4-8225153; E-mail: dmeiri@technion.ac.il

15 **Abstract**

16 In T-cell acute lymphoblastic leukemia (T-ALL) more than 50% of cases display autoactivation of Notch1
17 signaling, leading to oncogenic transformation. We have previously identified a specific chemovar of
18 Cannabis that induces apoptosis by preventing Notch1 maturation in leukemia cells. Here, we isolated
19 three cannabinoids from this chemovar that synergistically mimic the effects of the whole extract. Two
20 were previously known, Cannabidiol (CBD) and Cannabidivarin (CBDV); whereas the third cannabinoid,
21 which we termed 331-18A, was identified and fully characterized in this study. We demonstrated that
22 these cannabinoids act through Cannabinoid receptor type 2 and TRPV1 to activate the integrated stress
23 response pathway by depleting intracellular $Ca^{2+}$. This is followed by increased mRNA and protein
24 expression of ATF4, CHOP and CHAC1, which is hindered by inhibiting the upstream initiation factor
25 eIF2α. The increased abundance of CHAC1 prevents Notch1 maturation, thereby reducing the levels of
26 the active Notch1 intracellular domain, and consequently decreasing cell viability and increasing
27 apoptosis. Treatment with the three isolated molecules resulted in reduced tumor size and weight in-vivo
28 and slowed leukemia progression in mice models. Altogether, this study elucidated the mechanism of
29 action of three distinct cannabinoids in modulating the Notch1 pathway, and constitutes an important step
30 in the establishment of a new therapy for treating *NOTCH1*-mutated diseases and cancers such as T-ALL.

## Introduction

T-cell acute lymphoblastic leukemia (T-ALL) is an aggressive cancer, characterized by immature T-lymphoblasts (*1*, *2*). In over 50% of cases, activating mutations in *NOTCH1* were identified, generating much interest in targeting the Notch1 signaling pathway in this disease (*3–5*). The Notch1 protein is a single-pass transmembrane receptor that is expressed on the plasma membrane. It regulates evolutionarily conserved signaling that controls developmental processes, cell fate determination and tissue homeostasis. It is a member of the Notch receptor family, which consists of four receptors (Notch1-4) in humans (*4*, *6*). The Notch1 receptor-signaling pathway is activated through a series of proteolytic cleavages at three different sites (S1–S3). S1 cleavage is carried out by a Furin-like convertase in the trans-Golgi apparatus, resulting in a heterodimeric receptor that is transported to the membrane where it can bind ligands from a neighboring cell. Upon binding of a ligand, cleavage is performed at the next site and the activation of the Notch1 receptor-signaling pathway is initiated, enabling the cleavage of S3 in the transmembrane region that causes the release of the Notch1 intracellular domain (NICD), which translocates to the nucleus where it promotes transcription of target genes involved in cell growth (*7*).

Aberrant Notch1 activity is associated with many other leukemia types and other cancers, including prostate, lung, ovarian, and renal (*8–12*). A new and promising emerging field in cancer treatment is medical Cannabis and its unique active compounds, the phytocannabinoids. Phytocannabinoids affect the body by means of the endocannabinoid system (eCBS), a ubiquitous neuromodulatory signaling system that has widespread functions throughout the body. Notable eCBS receptors include cannabinoid receptor type 1 (CB1) and CB2, which belong to the family of G protein-coupled receptors, and transient receptor potential vanilloid type 1 (TRPV1), which is an ion channel (*13*). The eCBS participates in many physiological activities, including the regulation of $Ca^{2+}$ homeostasis (*14–16*).

Medical Cannabis is already commonly used by cancer patients for its palliative effects, it was shown to stimulate appetite while alleviating symptoms such as nausea, vomiting and pain (*17*). However,

55 accumulating evidence demonstrated phytocannabinoids directly affect tumor development in cell lines
56 and animal models by modulating key cell-signaling pathways (*18–20*). Studies demonstrated that purified
57 phytocannabinoids can inhibit proliferation, metastasis, and angiogenesis and exert pro-apoptotic effects
58 in a variety of cancer cell types such as lung, breast, prostate, skin, intestine, glioma, lymphoma, pancreas
59 and uterine cancers (*21–23*). In preclinical models, treatment with phytocannabinoids led to tumor
60 regression of different cancer types (*24*, *25*).
61 Concerning T-ALL, some studies using phytocannabinoids and their respective formulations (such as
62 Dronabinol) have shown anti-proliferative as well as proapoptotic effects in selected leukemia cell lines
63 and native leukemia blasts cultured *ex-vivo* (*26–28*). Nevertheless, the mechanisms of phytocannabinoid-
64 mediated antitumor effects are not yet fully understood. Most of the studies that examined the anti-cancer
65 effects of Cannabis have focused mainly on the two major phytocannabinoids (−)-*trans*-$\Delta^9$-
66 tetrahydrocannabinol ($\Delta^9$-THC) and Cannabidiol (CBD), but these are just two of more than 140 different
67 phytocannabinoids that have been identified in different Cannabis chemovars (*29*, *30*).
68 We have previously demonstrated that different Cannabis extracts with unique phytocannabinoid
69 compositions impaired the survival and proliferation of specific cancer cell lines, suggesting that the effect
70 of a particular Cannabis extract on a specific cancer cell line relies on its chemical composition (*31*).
71 Following this framework, we successfully matched a specific CBD-rich Cannabis extract to T-ALL
72 leukemia cells that harbor a *NOTCH1* mutation (*32*). In the present study, we investigated which specific
73 metabolites in the whole extract are responsible for T-ALL elimination, and elucidated the molecular
74 mechanism by which they mediate their antitumor effects in this type of cancer.

75 **Results**

76 We have previously shown a specific CBD-rich Cannabis extract selectively induces apoptosis in T-ALL
77 leukemia cell lines that harbor a *NOTCH1* mutation. Treatment led to accumulation of the full-length
78 immature form of Notch1 in the membrane, correspondingly with reduced NICD protein expression and
79 transcription activity (*32*).

80 **A combination of three phytocannabinoids induces apoptosis and reduces NICD expression**

81 The CBD-rich extract was more potent than pure CBD or other high-CBD chemovars (*32*). This implied
82 a specific combination of metabolites from the plant potentiate the full antitumor effect. Using a semi-
83 preparative HPLC, we separated the whole extract into four 10-minute retention time fractions (**Fig. 1A**).
84 A full list of the phytocannabinoids constituting each fraction is presented in supplementary table S1.
85 We assessed the effect of each fraction on the viability of MOLT-4 cells (fig. S1A) and found fraction 2
86 reduced viability to a similar extent as the whole extract. Further analysis revealed that out of the four
87 fractions, only fraction 2 induced apoptotic cell death (Fig. 1B), reduced the protein levels of the NICD
88 (Fig. 1C, D) and elevated the levels of cleaved caspase-3 (Fig. 1D). Thus, we excluded all the
89 phytocannabinoids present in the other three fractions, such as $\Delta^9$-THC in fraction 3.

90 To pinpoint the active phytocannabinoids in fraction 2, we further separated this fraction into individual
91 phytocannabinoids using centrifugal partition chromatography (CPC) followed by semi-preparative
92 HPLC (C1-C5 in Fig. 1E). We identified the specific compounds in the isolated peaks (Supplementary
93 table S2), C2 was identified as cannabidivarin (CBDV) and C5 as CBD. C3 and C4 were identified as
94 Cannabidiolic acid (CBDA), the precursor to CBD, and as CBD-C4, respectively; but their
95 concentrations were very low. C1 was identified as 331-18A, a phytocannabinoid first identified by our
96 team in decarboxylated CBD-rich Cannabis chemovars (*29*), we characterized 331-18A using ESI-
97 LC/MS/MS as having a deprotonated m/z of 331.2279 and MS/MS fragments resembling those of CBD

98 with the addition of one hydroxyl group. To confirm the identification, the purity of the three isolated
99 compounds was determined by UHPLC/UV (fig. S2A-C).

100 Here, we further elucidated the chemical structure of 331-18A by nuclear magnetic resonance (NMR)
101 with CBD as the reference (Supplementary Fig. S3 and table S3). The NMR data of CBD was in close
102 agreement with the literature (*33*). The spectra of CBD and 331-18A were very similar with the exception
103 of the disappearance of the external double bond ($C_8$-$C_{10}$) and the appearance of a tertiary alcohol instead.
104 The absolute stereochemistry of 331-18A was confirmed by specific rotation determination with a
105 polarimeter in which 331-18A showed $[\alpha]^{20}_D$ −56.85 which is comparable with the $[\alpha]^{20}_D$ −64.16 of both
106 the CBD that was isolated from the fraction (C5) and a commercial standard of CBD. These results
107 suggested that similarly to CBD, the two substituents at positions 1 and 6 of the cyclohexene ring are in
108 a *trans* configuration (Fig. 1F).

109 To examine the cytotoxic properties of the isolated compounds and their combinations on MOLT-4 cells,
110 the isolated phytocannabinoids were prepared in the same amounts and proportion as observed in the
111 whole extract; for example, if 1 μg of the whole extract contained 50% CBD, we used 0.5 μg of the purified
112 CBD and 1 μg of the whole extract in the respective treatments. Compared to the whole extract, the
113 phytocannabinoids 331-18A and CBDV alone did not induce apoptosis or had minor effects on the cells,
114 and CBD alone induced only 55% cell death compared to the whole extract (Fig. 1G). When CBD was
115 combined with either 331-18A or CBDV, the percent of apoptotic cells increased to 58% and 61%,
116 respectively. The combination of all three phytocannabinoids led to the greatest cytotoxic effect and only
117 this combination was comparable to the whole extract (88.29% ± 4.31% and 93.85% ± 1.64%,
118 respectively). We further evaluated the effect of the three phytocannabinoids separately or in different
119 combinations on the protein expression of NICD (Fig. 1H-I) and found that all combinations of

phytocannabinoids led to a significant reduction in NICD expression, but only when all the three were combined, NICD levels decreased to the same extent as with the whole extract.

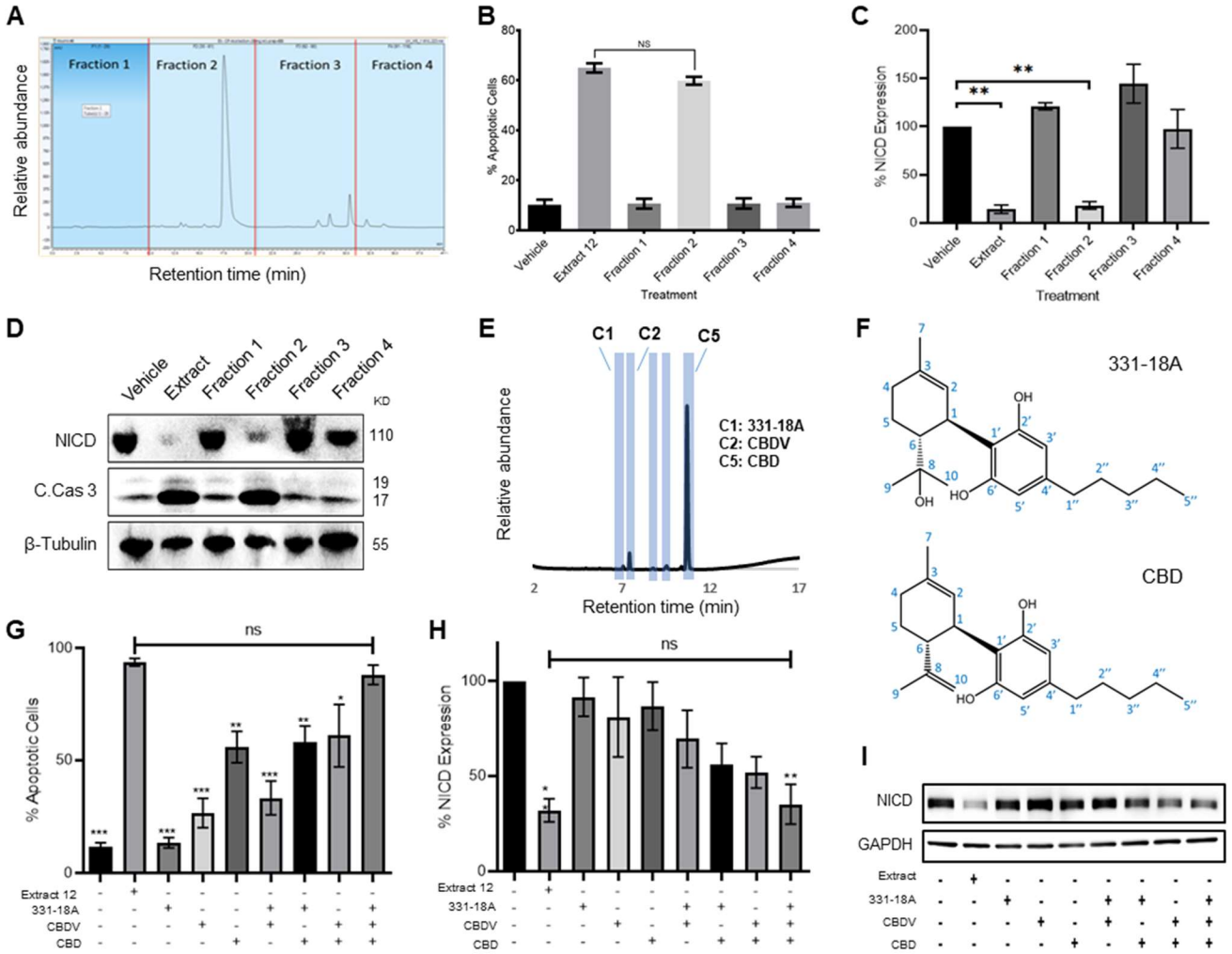


**Fig. 1. Identifying specific phytocannabinoids responsible for the cytotoxic effect of the whole extract.** (**A**) A semi-preparative HPLC-UV chromatogram of the whole extract showing the four fractions collected every 10 minutes. (**B-D**) MOLT-4 cells were treated with either vehicle, whole extract or fractions 1-4 (3 µg/mL) and (B) apoptosis was analyzed after 24 h (N=3) via Annexin V/PI, (C-D) NICD and cleaved caspase-3 (C. Cas. 3) expressions were evaluated (N=3) after 3 h with β-tubulin as the loading control. A representative blot is shown. (**E**) UHPLC/UV chromatogram of fraction 2, the specific compounds constituting the fraction are marked (C1-C5). (**F**) Chemical structure and peak assignment of CBD and 331-18A according to $^{1}$H and $^{13}$C NMR. Atom numbering is according to the monoterpene numbering system. (**G-I**) MOLT-4 cells were treated with the whole extract (3 µg/mL) or with 0.06 µg/mL 331-18A, 0.06 µg/mL CBDV and 1.5 µg/mL CBD, their corresponding concentrations in the extract, and their different combinations. Cells were assessed for (G) apoptosis after 24 h (N=3) via Annexin V/PI assay and (H-I) NICD expression after 3 h (N=3) with GAPDH as the loading control. Results are presents as mean ± SEM and statistically analyzed with One-way ANOVA (*$p<0.05$, **$p<0.01$, ***$p<0.001$).

123 **331-18A, CBDV and CBD mediate their effect through CB2 and TRPV1 to trigger $Ca^{2+}$ flux**

124 Phytocannabinoids usually operate through specific cannabinoid receptors in the eCBS. To elucidate
125 which endocannabinoid receptors mediate the antitumor effect, we first evaluated in MOLT-4 cells the
126 mRNA expression of *CNR1* and *CNR2* (for CB1 and CB2, respectively), as well as G protein-coupled
127 receptor 55 (*GPR55)*, *TRPV1*, Transient receptor potential cation channel, subfamily A, member 1
128 (*TRPA1*) and Transient receptor potential cation channel subfamily M (melastatin) member 8 (*TRPM8*),
129 (**Fig. 2A**). The ΔCT results showed low expression for *CNR1*, *TRPA1* and *TRPM8*, medium expression
130 for *CNR2* and *GPR55*, and high expression for *TRPV1*. We tested antagonists for those receptors that had
131 either high or medium expression: TRPV1 (AMG9810), CB2 (AM630 or SR-144,528), GPR55 (CID),
132 and general Gq GPCR (BIM-46187) as a control, and evaluated whether they were able to rescue NICD
133 expression upon treatment with the whole extract (fig. S4A-B). Only the CB2 and TRPV1 antagonists
134 rescued the expression of NICD upon treatment with the whole extract, therefore we tested whether they
135 were able to rescue NICD expression after treatment with the combination of 331-18A, CBDV and CBD
136 (Fig. 2B-C). The CB2 antagonist rescued the expression from 56% to 87%, and the TRPV1 antagonist
137 rescued NICD expression to 100% by itself.

138 TRPV1 is a $Ca^{2+}$ channel and eCBS receptors are known to trigger $Ca^{2+}$ flux (*15*, *16*). Therefore, as the
139 next step we tested the effect of the three cannabinoids on cytosolic $Ca^{2+}$ levels. We used the Fluo-4
140 calcium probe to measure the effect of 331-18A, CBDV and CBD combination on MOLT-4. Each of the
141 molecules separately caused some elevation in $Ca^{2+}$, but only their combination had an effect on $Ca^{2+}$ to
142 the same extent as the whole extract (Fig. 2D). We tested $Ca^{2+}$ levels when cells were pretreated with the
143 antagonists to CB2 and TRPV1. Both antagonists inhibited the elevation in response to the whole extract
144 (Supplementary fig. S3C, D). When 331-18A, CBDV and CBD were tested separately with antagonists
145 to either CB2 or TRPV1 (Fig. 2E), CB2 but not TRPV1 antagonist diminished 331-18A induced $Ca^{2+}$

146 increase, indicating this cannabinoid exerts its effect through CB2, while both antagonists significantly
147 decreased the $Ca^{2+}$ elevation by CBDV and CBD. Next, we assessed whether inhibition of the receptors
148 rescues MOLT-4 cells from the cytotoxic properties of the cannabinoid combination (Fig. 2F). Treatment
149 with the inhibitors by themselves, separately or both together, did not induce MOLT-4 cell death. Upon
150 treatment with the combination of 331-18A, CBDV and CBD, inhibition of CB2 only partially rescued
151 the cells from treatment-induced apoptosis, reducing the apoptotic rate from 75% of the combination-

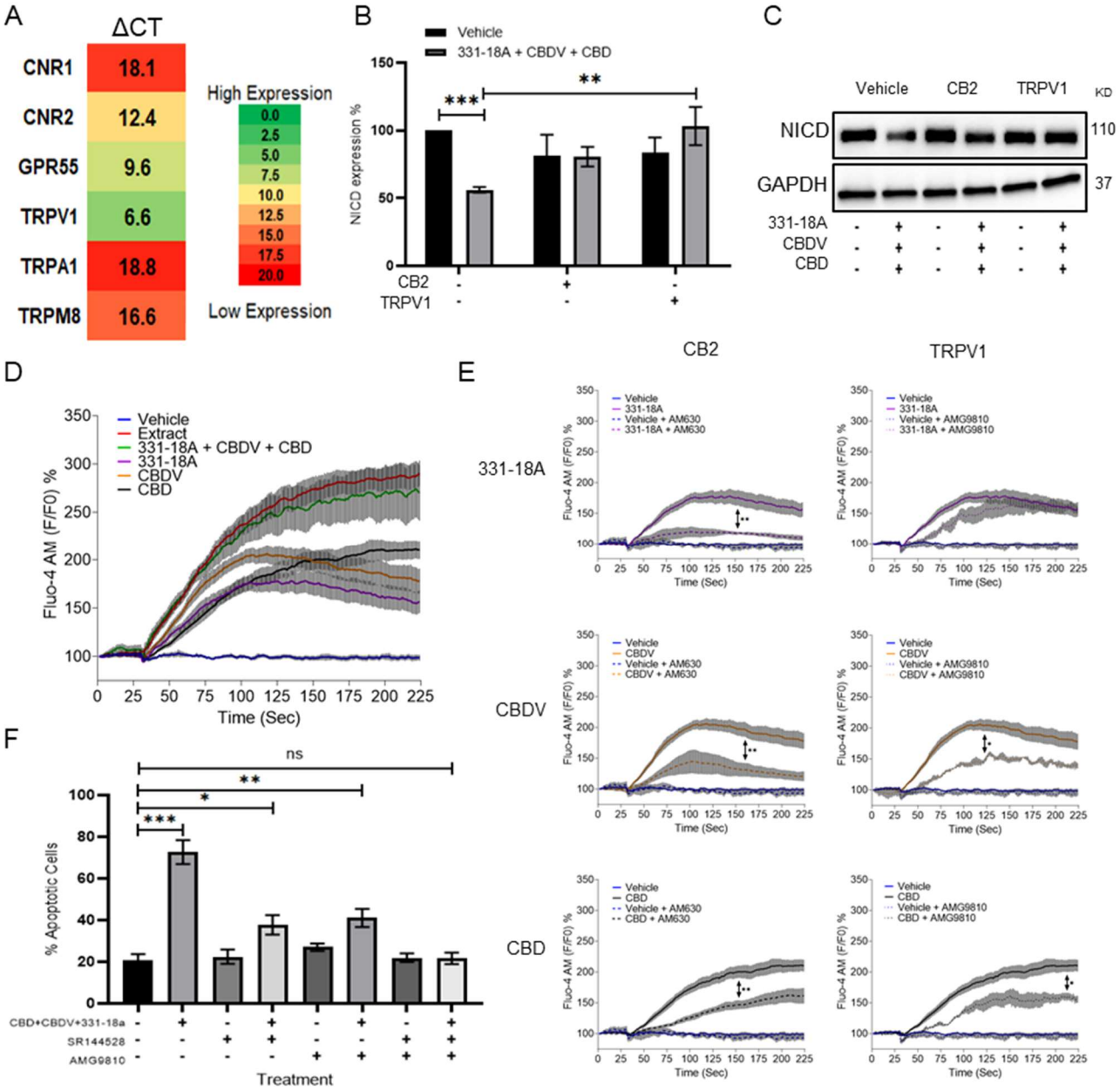

**Fig. 2. 331-18A, CBDV and CBD mediate their effect through CB2 and TRPV1**. (**A**) The mRNA levels of receptors *CNR1* (CB1), *CNR2* (CB2), *GPR55*, *TRPV1*, *TRPA1* and *TRPM8* were evaluated by qRT-PCR. Gene expression levels were calculated as ΔCT normalized to *GUSB* housekeeping gene. Results are presented as mean expression of three biological replicates. High ΔCT values indicate low receptor expression. (**B**) MOLT-4 cells were pretreated with 50 μM antagonist to CB2 (AM630) or TRPV1 (AMG9810) for 30 min, then treated with the combination of the three cannabinoids for 3 h. NICD expression was evaluated by western blot (N=3) with GAPDH as the loading control and statistically analyzed with an unpaired student's t-test (**p<0.01, ***p<0.001). (**C**) Representative blots of B. (**D**) Calcium release by MOLT-4 cells was measured with the Fluo-4 calcium probe immediately following treatment with either vehicle, whole extract, a combination of 331-18A, CBDV and CBD, and each cannabinoid separately. The calcium curves represent an average of three independent experiments. (**E**) Reduction of each phytocannabinoid-induced calcium release by pretreatment with 50 μM of antagonist to CB2 (AM630) or TRPV1 (AMG9810) for 30 min. The calcium curve for each compound is given again in this graph to compare the effects with the antagonists (N=3, two-way ANOVA, *p<0.05, **p<0.01). (**F**) MOLT-4 cells were pretreated with 50 μM antagonist to CB2 (SR-144,528) or TRPV1 (AMG9810) or both for 30 min, then treated with the combination of the three cannabinoids or left untreated. Apoptosis was analyzed after 24 h (N=3) by Annexin V/PI. Results are presented as mean ± SEM and statistically analyzed with one-way ANOVA (*p<0.05, **p<0.01, ***p<0.001).

152 treated cells to 40%. However, the apoptotic rate was still significantly higher than that of the untreated
153 control. Inhibition of TRPV1 only also partially rescued the cells, to ~50%, but again the apoptotic rate
154 remained significantly increased relative to the untreated control. Inhibition of both CB2 and TRPV1
155 simultaneously rescued the cells from treatment-induced apoptosis, confirming the effect of the three
156 cannabinoids is mediated through both receptors.

157 **Notch1 downregulation by cannabinoids is mediated through the integrated stress response**
158 **pathway**

159 To elucidate the mechanism by which the Notch1 pathway is down-regulated following treatment, we
160 used RNA-seq analysis to measure and compare the gene expression profile of MOLT-4 cells after 3 hours
161 of treatment with either vehicle or the whole extract (**Fig. 3A**). A list of the ten most increased- and
162 decreased-abundance genes following treatment is presented in supplementary table S4. ChaC
163 glutathione-specific γ-glutamylcyclotransferase 1 (*CHAC1*), a negative regulator of the Notch signaling
164 pathway (*34*), was identified as the second most increased-abundance gene. CHAC1 acts by inhibiting the
165 furin-like cleavage of Notch1, preventing the formation of the mature form of Notch1 (*35*), as we have

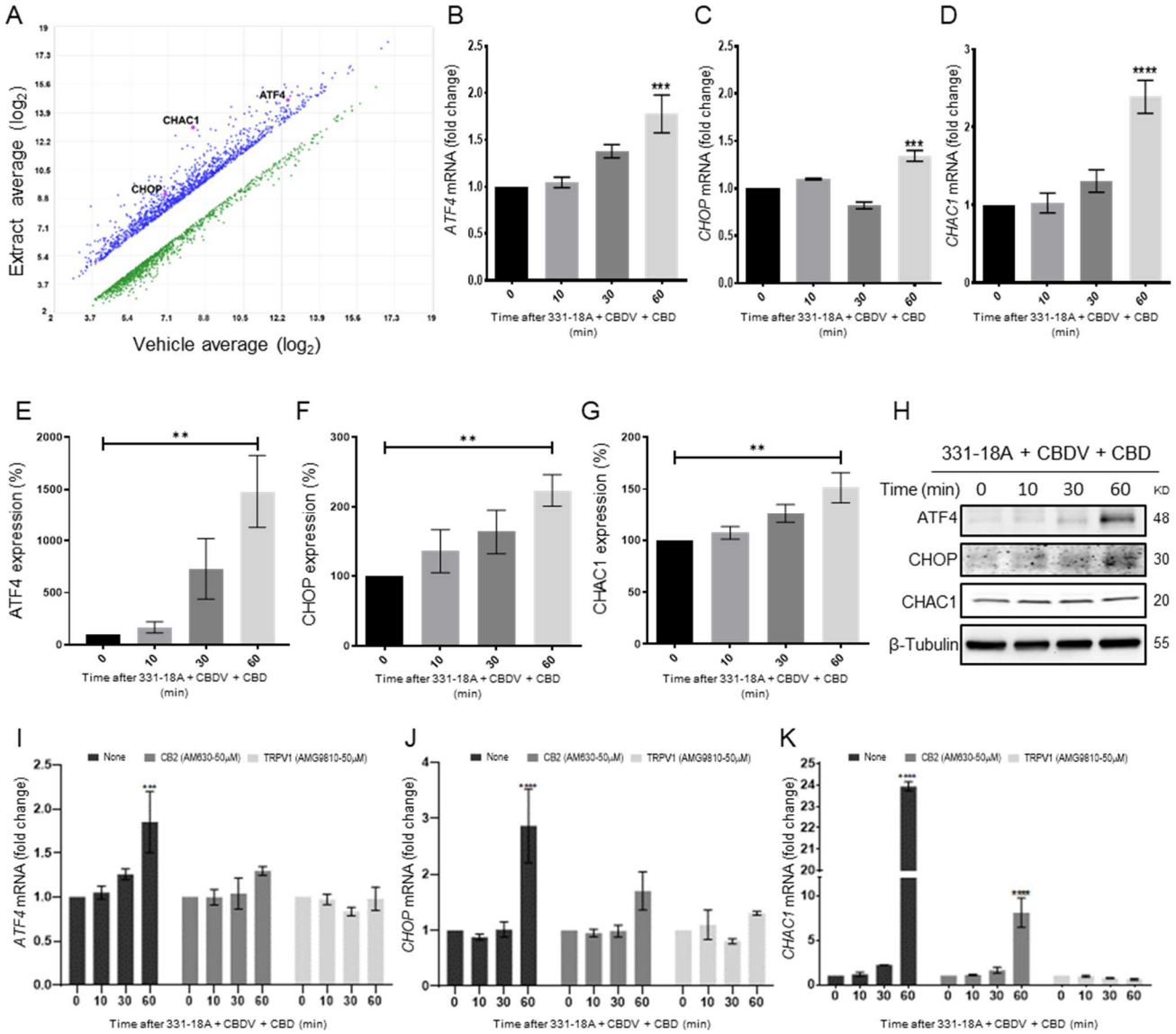


**Fig. 3. Notch1 downregulation by 331-18A, CBDV and CBD combination is mediated via ATF4-CHOP-CHAC1 signaling pathway.** (**A**) MOLT-4 cells were treated for 3 h with either vehicle or the whole Extract (3 µg/mL) and an RNA-seq (affymetrix) scatter plot presents the differential expression; the increased abundance genes *CHAC1*, *CHOP* and *ATF4* are marked (N=3). (**B-D**) MOLT-4 cells were treated for 3 h with 331-18A, CBDV and CBD combination (N=3), the mRNA expression of *ATF4*, *CHOP* and *CHAC1* genes was evaluated with qRT-PCR at different time points (0-60 min). Differences are presented as fold-change ± SEM and statistically analyzed with one-way ANOVA (***p<0.001, ****p<0.0001). (**E-G**) MOLT-4 cells were treated as in B-D and the protein expression of ATF4, CHOP and CHAC1 were evaluated with β-tubulin as the loading control. Intensity analysis was performed on three independent experiments (N=3) and statistically analyzed with an unpaired Student's *t*-test (**p<0.01). (**H**) Representative blots. (**I-K**) Analysis of ATF4, CHOP and CHAC1 mRNA expression at different time points following pretreatment with CB2 and TRPV1 antagonists for 30 min and then treatment with the cannabinoid combination (N=3), analyzed with two-way ANOVA (***p<0.001, ****p<0.0001).

166

167 previosly demonstrated upon treatment with the whole extract (*32*). C/EBP homologous protein (*CHOP*)
168 and Activating transcription factor 4 (*ATF4*), ER-stress signaling pathway markers that are upstream to
169 *CHAC1* (*36*), had also a significant increase in their abundance. We confirmed the RNA-seq results by
170 qRT-PCR showing that the mRNA of *ATF4*, *CHOP* and *CHAC1* is indeed significantly increased after
171 treatment with a combination of 331-18A, CBDV and CBD (Fig. 3B-D, respectively) or the whole extract
172 (fig. S3E-G). A significant increase was apparent 60 min after treatment. Using specific antibodies to
173 ATF4, CHOP and CHAC1, we verified the protein expression level of all three was also significantly
174 increased at 60 min after treatment (Fig. 3E-H). The protein expression levels of CHAC1 in MOLT-4 cells
175 were also significantly increased upon treatment with the whole extract (fig. S3H, I).
176 To further understand the mechanism, we evaluated how pretreatment with antagonists to the cannabinoid
177 receptors through which 331-18A, CBDV and CBD exert their effect, CB2 and TRPV1, affected *ATF4*,
178 *CHOP* and *CHAC1* expression following treatment (Fig. 3I-K). Inhibition of CB2 reduced the treatment-
179 induced increase in mRNA expression, but a trend of increase for ATF4 and CHOP remained at 60
180 minutes, and CHAC1 expression was significantly increased. Inhibition of TRPV1 rescued from
181 treatment-induced induction of all three targets. Similar effects were found when pretreatment with
182 antagonists to CB2 and TRPV1 was followed by treatment with the whole extract (fig. S3J-L); and the
183 increase in the expression levels of CHAC1 protein was abolished when MOLT-4 cells were treated by
184 either antagonist (fig. S3M). These results demonstrate that CB2 and TRPV1 participate in inducing
185 CHAC1 expression and preventing Notch1 maturation, resulting in a decrease in NICD release and cell
186 death.
187 We therefore speculated that the combination of the three cannabinoids caused the activation of ATF4-
188 CHOP-CHAC1 signaling by $Ca^{2+}$ depletion and ER-stress (*37*). To further verify the role of ATF4-CHOP-
189 CHAC1 signaling in mediating the downregulation of the Notch1 pathway, we inhibited the activity of

190 the upstream target eukaryotic Initiation Factor-2α (eIF2α) in MOLT-4 cells using integrated stress
191 response inhibitor (ISRIB), which inhibits the activity of eIF2α without affecting its phosphorylation (*38*)
192 (fig. S5A-B). Then, we treated the cells with either vehicle or the combination of the cannabinoids. After
193 24 hours, blocking the activity of eIF2α prevented the cytotoxic effect of 331-18A, CBDV and CBD
194 combination (**Fig. 4A**) or of the whole extract (fig. S5C). Moreover, eIF2α inhibition prevented the
195 reduction in NICD expression upon treatment with either the whole extract (fig. S5D-E) or the cannabinoid
196 combination (Fig. 4B-C). Inhibition of eIF2α also rescued the cells from the induced increase in the
197 mRNA expression of ATF4, CHOP and CHAC1 upon treatment with the combination of the cannabinoids

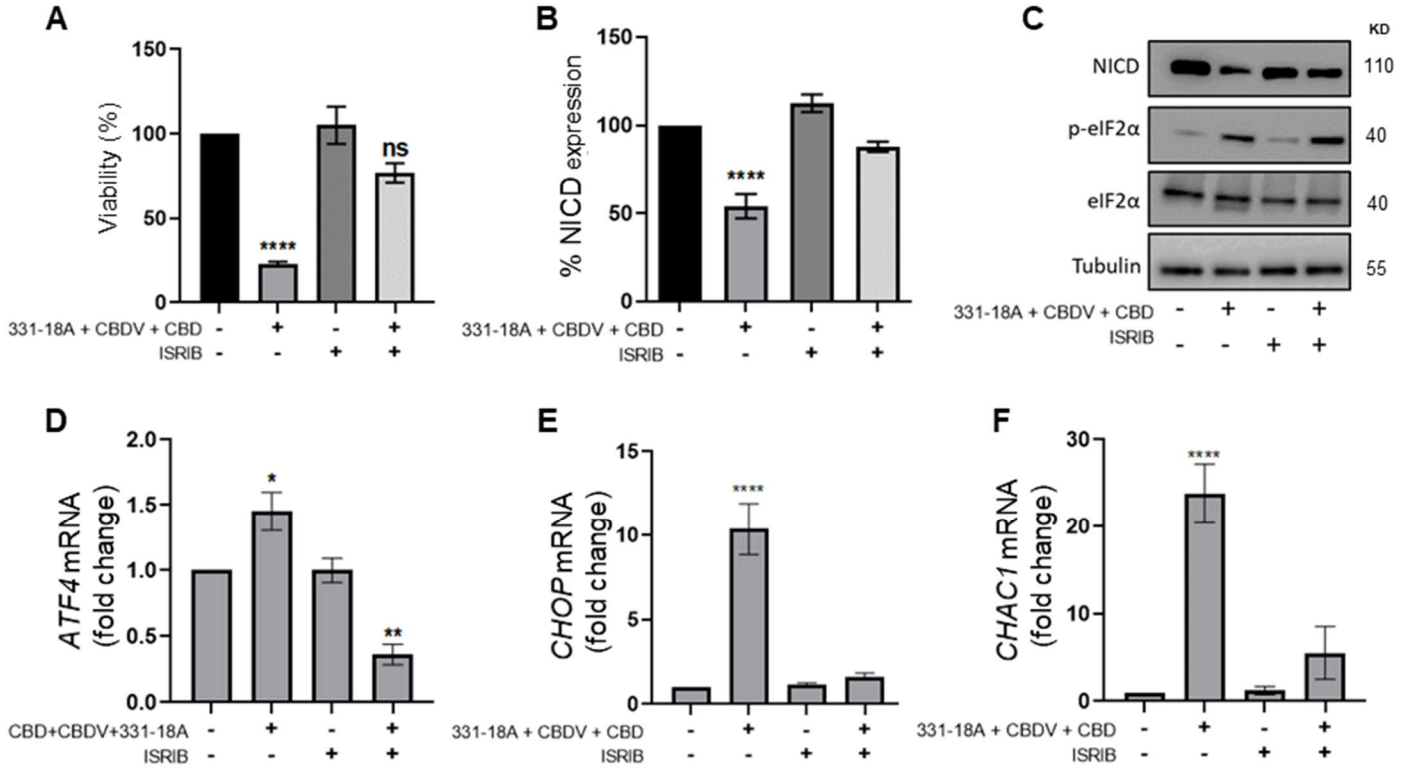


**Fig. 4. 331-18A, CBDV and CBD combination activates eIF2α.** MOLT-4 cells were pretreated for 30 min with the eIF2α inhibitor ISRIB (150 μM) or left untreated, then treated with vehicle or the combination of 331-18A, CBDV and CBD for 3 h. (**A**) Viability after 24 hrs was assessed with XTT (N=3). (**B**) NICD protein expression was assessed (N=3) with β-Tubulin as the loading control (unpaired Student's *t*-test, *p<0.05). (**C**) A representative image also showing the protein levels of phosphorylated eIF2α ($Ser^{51}$) and total eIF2α. (**D-F**) *ATF4*, *CHOP* and *CHAC1* gene expression was assessed via qRT-PCR 4 hrs after treatment (N=3). Results are presented as mean ± SEM and statistically analyzed with one-way ANOVA (****p<0.0001).

198 (Fig. 4D-F). Thus, inhibition of the integrated stress response pathway, eIF2α-ATF4-CHOP-CHAC1
199 signaling, rescued MOLT-4 cells from the cytotoxic effect of the combination of the three cannabinoids
200 and prevented the reduction in NICD expression, as well as the increased transcription of ATF4, CHOP
201 and CHAC1 upon treatment.

202 To further investigate the interaction between 331-18A,CBDV and CBD, we assessed their effect on the
203 viability of MOLT-4 cells in different relative proportions. First we tested the ability of each seaparate
204 cannabinoid to inhibit the proliferation of MOLT-4 cells in doses ranging 0-2 μg/ml (**Fig. 5A**), which is
205 below and above the overall concentration for which we found an effect for the cannabinoid combination.
206 331-18A and CBDV affected viability from a dose of 1 μg/ml and CBD from a dose of 0.5 μg/ml. Next,
207 we calculated the combination index of every pair and all three cannabinoids in concentrations ranging
208 from 0-2 μg/mL (Fig. 5B-E). The most synergistic area is displayed in red. We calculated the total synergy
209 score for the combination of all three cannabinoids relative to the pairwise combinations (Fig. 5F).
210 According to Highest Single Agent (HSA) reference model(*39*), a combination of CBDV with either 331-
211 18A or CBD results in a likely antagonistic interaction (score < -10), a combination of 331-18A and CBD
212 results in a likely additive interaction (score from -10 to 10), and only the combination of all three
213 cannabinoids is likely synergistic (score > 10, Fig. 5G).

214 **Inhibition of cancer progression in-vivo by 331-18A, CBDV and CBD combination**

215 We further evaluated the anti-tumor properties of the three cannabinoids using several mouse models. The
216 first model was a subcutaneous tumor model for which we have already demonstrated the effectivity of
217 the whole extract (*32*). We engrafted subcutaneously Nonobese diabetic-severe combined
218 immunodeficiency (NOD/Scid) mice with MOLT-4 cells, then treated with vehicle only or the
219 combination of the cannabinoids from when tumors reached a volume of 100 $mm^3$ (day 7), on alternating
220 days, for a duration of four weeks. Treatment with a combination of 331-18A, CBDV and CBD

221 significantly inhibited tumor growth (**Fig. 6A-C**). Significant differences were apparent approximately 3

222 weeks after treatment started (Fig. 6A), and at the endpoint, 34 days from the injection of cells, the average

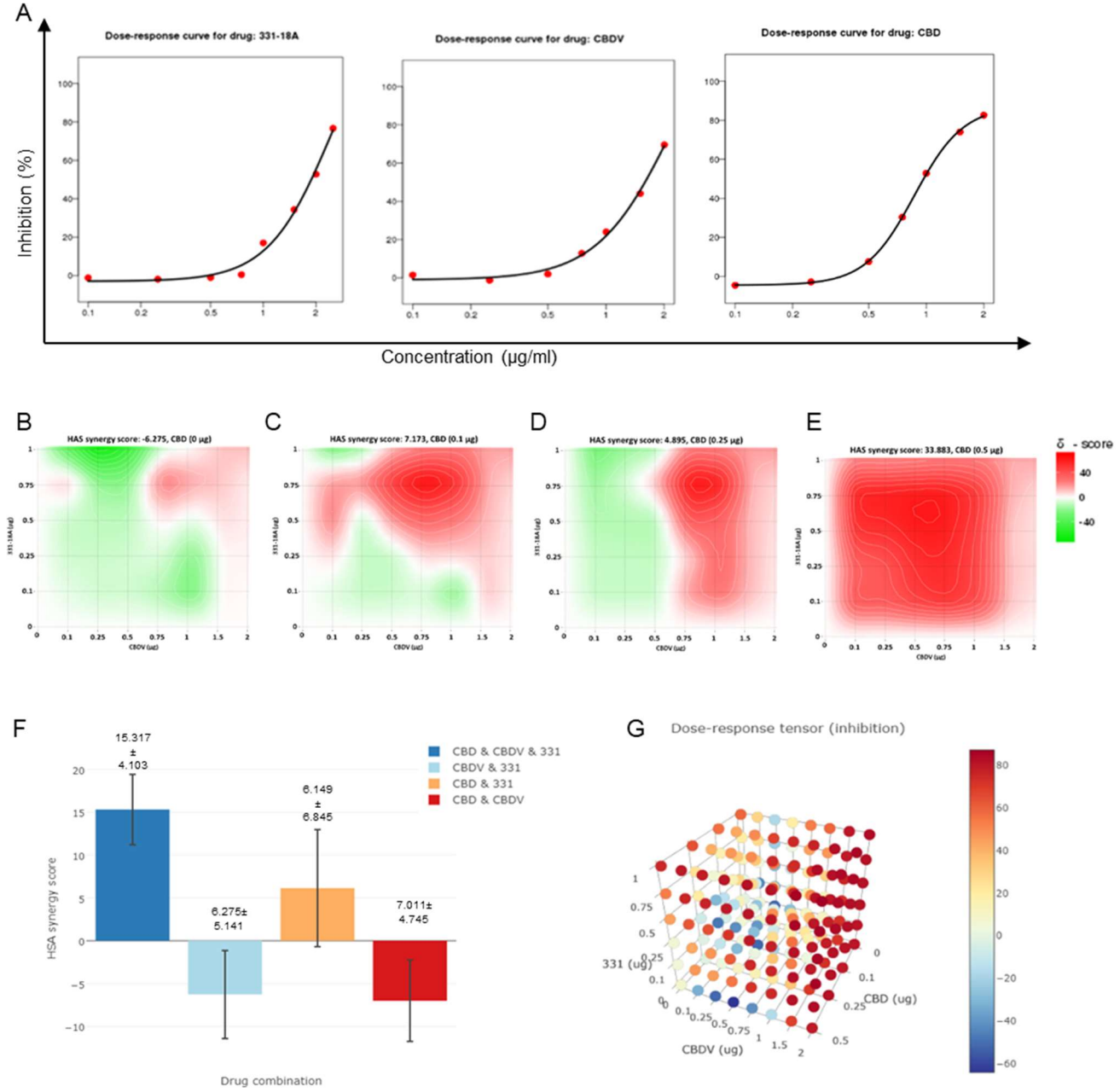


**Fig. 5. All three cannabinoids must be combined for a synergistic effect**. (**A**) MOLT-4 cell death (N=3) was assessed by XTT following treatments with concentrations ranging 0-2 µg/ml and a dose-response curve for each cannabinoid separatly was plotted. (**B-E**) Synergy distribution for different ratios of cannabinoids was calculated by HSA model with SynergyFinder web application (v 2.0), representative dose-response matrices are presented for CBD at (B) 0, (C) 0.1, (D) 0.25 and (E) 0.5 µg/ml. (**F-G**) Best synergy scores according to HSA model presented for the triple combination relative to the two-cannabinoid combinations.

weight of tumors was significantly lower in the treated group compared to the control group (Fig. 6B). Excised tumors (Fig. 6C) were analyzed for their cannabinoid content according to a method recently developed by our group for biological tissues (*40*). Using ESI-LC/MS, we identified and quantified each of the three cannabinoids in the tumors [16.0 ± 6.7, 22.3 ± 10.4 and 265.8 ± 109.7 ng/g for CBDV, 331-18A and CBD, respectively (average ± S.E.M., N=3)]. Notably, the ratio of the cannabinoids analyzed in the tumors was similar to the ratio given to the mice in the treatment protocol. In addition, a significant decrease was observed in NICD expression in the tumors treated with the cannabinoids (Fig. 6D). To assess possible toxicity, the body weight of the mice was monitored throughout the experiment (Fig. 6E). There were no significant differences in the average weight of mice in the control group and the treatment group.

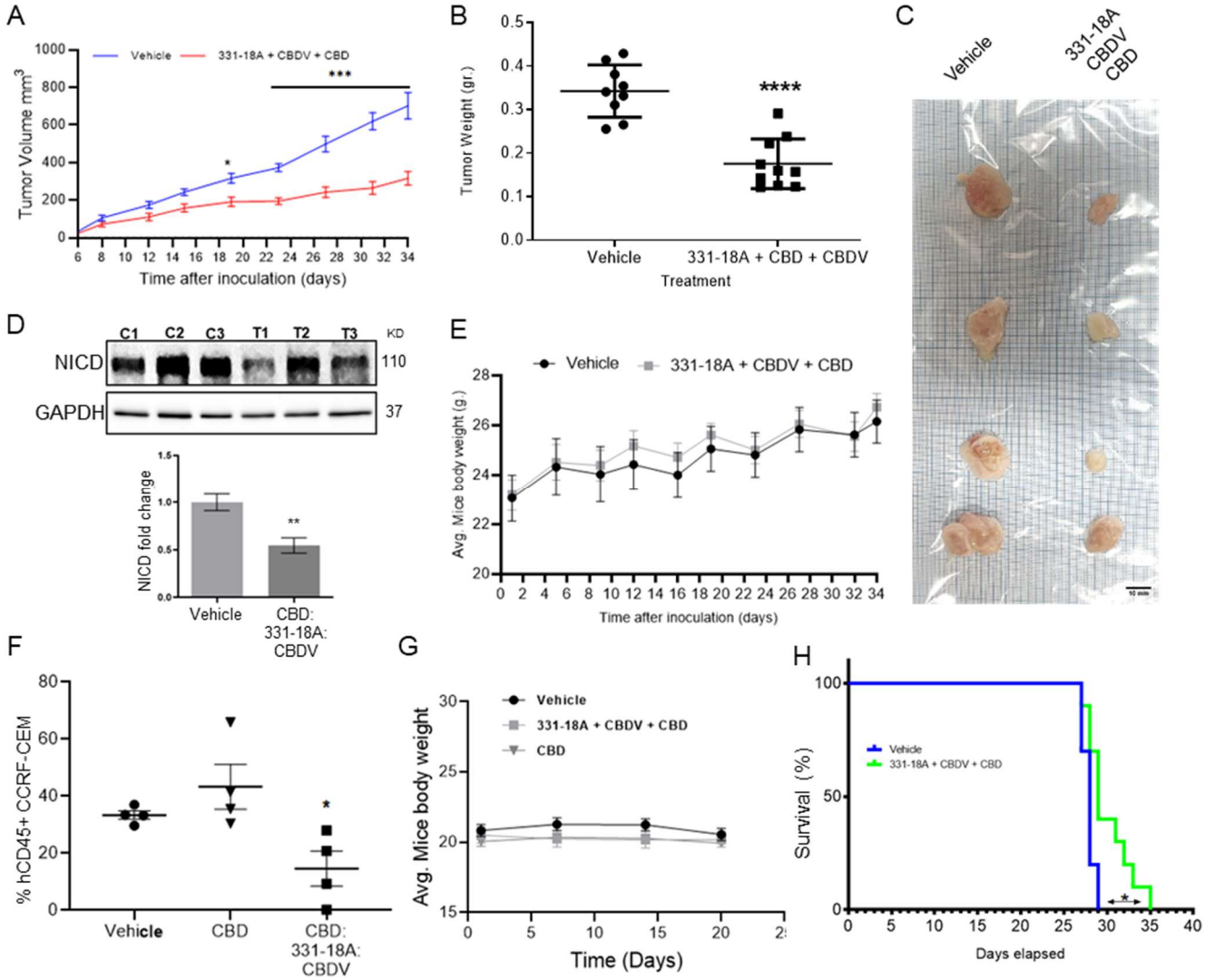

**Fig. 6. Inhibition of cancer progression in-vivo by a combination of 331-18A, CBDV and CBD**. (**A**) Female NOD/Scid mice (N=4-5/group, two independent experiments) were engrafted subcutaneously with $1\times10^6$ MOLT-4 cells. After seven days, the mice were randomly divided into two groups and alternate-day treated intraperitoneally with either vehicle or a combination of 331-18A (1.11 mg/kg), CBDV (1.11 mg/kg) and CBD (17.77 mg/kg). Ectopic tumor volume was measured using a vernier caliper and calculated according to the formula (length × width$^2$) × 0.5. The average difference between groups was statistically analyzed by Bonferroni's multiple comparisons test (*p<0.05, ***p<0.001). (**B**) After 34 days of treatment, the mice were sacrificed and tumors were excised and weighed (N=9). The difference in the weights of the tumors between treatment groups was statistically analyzed by unpaired Student's *t*-test (****p<0.0001). (**C**) Representative photograph of excised tumors. (**D**) A representative blot (*top*) and fold change (*bottom*) of NICD protein expression in excised tumors at day 34 after treatment with either vehicle (C) or a combination of the three cannabinoids (T), with GAPDH as the loading control. Data are presented as mean ± SEM (N=3) and statistically analyzed by unpaired Student's *t*-test (**p<0.01). (**E**) Body weight (grams) in vehicle- and cannabinoids-treated mice. (**F**) Female NSG mice were intravenously injected with $1\times10^6$ human CCRF-CEM cells. Mice were randomly divided into three groups (N=5/group) and treated intraperitoneally daily for five days, then left untreated for two days before starting another cycle, for a period of three weeks. Treatment groups were vehicle, pure CBD (30 mg/kg), and a combination of CBD (26.67 mg/kg), CBDV (1.67 mg/kg) and 331-18A (1.67 mg/kg) at the same overall concentration as pure CBD. After 24 days, the percentage of hCD45+ cells in the bone marrow was measured with flow cytometry and statistically analyzed by unpaired student's t-test (*p<0.05). (G) Body weight (grams) in vehicle- and cannabinoids-treated mice. (H) Survival analyses after CCRF-CEM injection followed by treatment with either vehicle or the cannabinoid combination (N=10/group), statistical differences were calculated with the Log-rank (Mantel-Cox) test (*p<0.05).

233 Next, we assessed the cannabinoids using an intravenous model which better resembles leukemogenesis
234 (*41*, *42*). We engrafted NOD-SCID IL2rγ-null (NSG) mice that are a better host for human immune cells
235 with CCRF-CEM, Notch1 mutated T-ALL cells. The mice were treated with a combination of the three
236 cannabinoids, and to verify the need for the combination, one group was also treated with pure CBD in
237 the same overall dose. At the endpoint of the experiment, the amount of human CD45+ cells detected in
238 the bone marrow (BM) was significantly decreased in the mice treated with the combination of the three
239 cannabinoids compared to the control, and compared to pure CBD (Fig. 6F). In this model as well, there
240 were no significant differences in the average weight of the mice (Fig. 6G). The combination of 331-18A,
241 CBDV and CBD was as effective as the whole extract (fig. S6A-B). In addition, the administration of the
242 cannabinoid combination significantly prolonged survival in treated mice compared to the survival of
243 vehicle-treated control mice (Fig. 6H), to a similar degree to the whole extract (fig. S6C).

244 To examine the clinical relevance, we utilized a patient-derived xenografts (PDX) model with primary
245 cells from a T-ALL patient. After allowing 35 days from transplantation for leukemic cell establishment,
246 mice were treated for three weeks with either vehicle or whole extract containing the three cannabinoids.
247 In mice that were treated with the extract, we found a significant reduction in the burden of leukemia in
248 the bone marrow (fig. S7A), peripheral blood (fig. S7B) and spleen (fig. S7C). The weight of the spleen
249 was also significantly lower in extract-treated mice (fig. S7D, E). Treatment with the whole extract did
250 not affect the weight of the mice.
251

252 **Discussion**

253 Targeting Notch signaling components has generated much interest for its therapeutic potential. However,
254 so far efforts to develop treatments that target Notch signaling have been unsuccessful (*43*). Cannabis, in
255 its many forms, is already being prescribed to cancer patients all over the world, mainly as a palliative
256 treatment for the inhibition of nausea and emesis associated with chemotherapy, appetite stimulation, pain
257 relief and relief from insomnia (*17*). On top of that, recent studies have demonstrated that
258 phytocannabinoids also possess anti-cancer potential (*24*, *25*, *31*, *44–46*).
259 In the current study, we identified three unique phytocannabinoids that together selectively induce
260 apoptosis in Notch1 mutated leukemia cells: CBD, CBDV and the novel phytocannabinoid 331-18A. CBD
261 and CBDV are well-known and commercially available. However, to the best of our knowledge, the third
262 phytocannabinoid 331-18A, denoted in the literature as 6,12-dihydro-6-hydroxy-cannabidiol (*47*), has not
263 been previously identified in natural and/or decarboxylated Cannabis plants. We suggest that the need for
264 all three cannabinoids for the optimal anti-tumor effect demonstrates the critical importance of elucidating
265 the individual and polypharmacological effects of the entire molecular spectrum of Cannabis.
266 Although CBD by itself demonstrated some capacity to induce cell death, it was only when all three
267 cannabinoids were combined that the same extent of response was achieved as treating with the whole

268 extract. The Cannabis plant produces a vast array of over 140 phytocannabinoids and hundreds of other
269 components, but the full extent of their biological effects and interactions is still not completely
270 understood. Nevertheless, mounting evidence suggests that their combined effect as a whole is greater
271 than that of each separate compound (*48*, *49*). Recently, Blasco-Benito *et al*. (*50*), have shown that a $\Delta^9$-
272 THC-rich extract was much more potent than pure $\Delta^9$-THC in producing antitumor responses in both cell
273 culture and animal models of breast cancer. However, they were unable to identify the combinations of
274 compounds that were responsible for this increased potency. In previous publications by our group, we
275 showed that different CBD-rich Cannabis extracts, with equal amounts of CBD but varying concentrations
276 of other minor compounds, lead to diverse anticonvulsant effects in a mouse model of epilepsy (*29*), and
277 selective antitumoral effects in Notch1-mutated in T-ALL (*32*); suggesting the potential therapeutic
278 effects of other compounds in the extracts in addition to CBD.
279 A possible mechanism previously suggested to explain the difference between the effects of purified
280 phytocannabinoids versus full-spectrum extracts is the "entourage effect", where one compound may
281 synergize the activity and efficacy of another on the same target (*48*, *49*). This "entourage effect" was
282 postulated by Russo (*48*) based on a phenomenon observed in the eCBS by Ben Shabbat *et al*. (*51*). While
283 it is well-established for endocannabinoids, only very few studies demonstrated this for
284 phytocannabinoids. We showed here that the presence of small amounts of the minor cannabinoids 331-
285 18A and CBDV enhanced the effect of CBD by itself. Our success in isolating and characterizing a
286 minimal number of cannabinoids that achieve the same antitumor effect as the whole extract is a
287 significant advancement in the field of medical Cannabis and provides solid evidence for the “entourage
288 effect”.
289 Subsequent reports have expanded the notion of the "entourage effect" to polypharmaceutical and/or
290 polypharmacological effects, where several of the plant metabolites work simultaneously on the same

291 receptors, and/or when the same molecule has several different targets within the same system (*52–54*).
292 CBD has been shown to present complex signaling capabilities of many receptors in the extended eCBS.
293 Specifically, it was shown to have a weak affinity to CB2, and a strong affinity to many of the TRPV
294 family receptors, including TRPV1, TRPV2 and TRPV3 (*55*, *56*).
295 We suggest that the Notch1-mutated T-ALL cells are affected through the engagement of the eCBS
296 receptor CB2 and the channel TRPV1. More specifically, the known cannabinoids CBD and CBDV
297 affected both, while the novel 331-18A exerted its effect only through CB2. Following the stimulation of
298 the receptors, $Ca^{2+}$ is depleted from the ER and there is an increase in cytosolic $Ca^{2+}$ and activation of
299 eIF2α followed by ATF4-CHOP-CHAC1 signaling. Notably, the inhibition of eIF2α upstream to ATF4
300 rescued T-ALL cells from reduced NICD expression by treatment with 331-18A, CBDV and CBD
301 combination. The upregulation of CHAC1 inhibits the S1 furin-like cleavage of Notch1 at the Golgi
302 apparatus (*35*), leading to the arrival of immature Notch1 to the plasma membrane as we have previously
303 shown (*32*). This inhibition of the Notch1 pathway ultimately leads to apoptosis in T-ALL cells that rely
304 on mutated Notch1 for propagation (see schematic representation in Fig. 7).
305 The potential antitumor effects of cannabinoids through the Notch1 signaling pathway were previously
306 demonstrated in glioma, where THC induced the expression of p8 protein, upstream to ATF3/4 (*57*). The
307 activation of Notch signaling by ER stress was demonstrated in additional systems, including Alzheimer's
308 disease (*58*), polycystic ovary syndrome (*59*) and other types of cancer (*60*, *61*). A previous work that
309 focused on chronic lymphocytic leukemia suggested a role for ER stress in Notch1 cleavage and leukemia
310 cell death through the inhibition of proteasome activity (*62*). These findings suggest blocking Notch1
311 maturation through the eIF2α-ATF4-CHOP-CHAC1 pathway and inhibiting the S1 furin-like cleavage of
312 Notch1 have the potential to affect all types of activation mutations in Notch1, and also all four human
313 homologs of Notch (Notch1-4) (*35*, *63*).

We demonstrated the effectiveness of the whole extract and the combination of the cannabinoids in several *in-vivo* models. To validate the clinical relevance of our findings for patients, we tested the extract containing the three cannabinoids in an *in-vivo* PDX model (*64*, *65*) (fig. S7), and demonstrated treatment reduced leukemic burden. As medical Cannabis is already routinely prescribed to cancer patients, tailoring chemovars that contain the appropriate cannabinoids to T-ALL patients can provide them with optimal care that offers anti-cancer properties on top of the palliative ones. Our findings are potentially relevant for numerous diseases, as dysregulation of Notch signaling has been found in various other cancers including breast, prostate and colorectal; as well as in non-cancerous diseases (*8*, *9*, *12*). As such, they may pave the way for the establishment of new pharmacotherapies for the treatment of Notch1-dependent malignancies and other diseases.

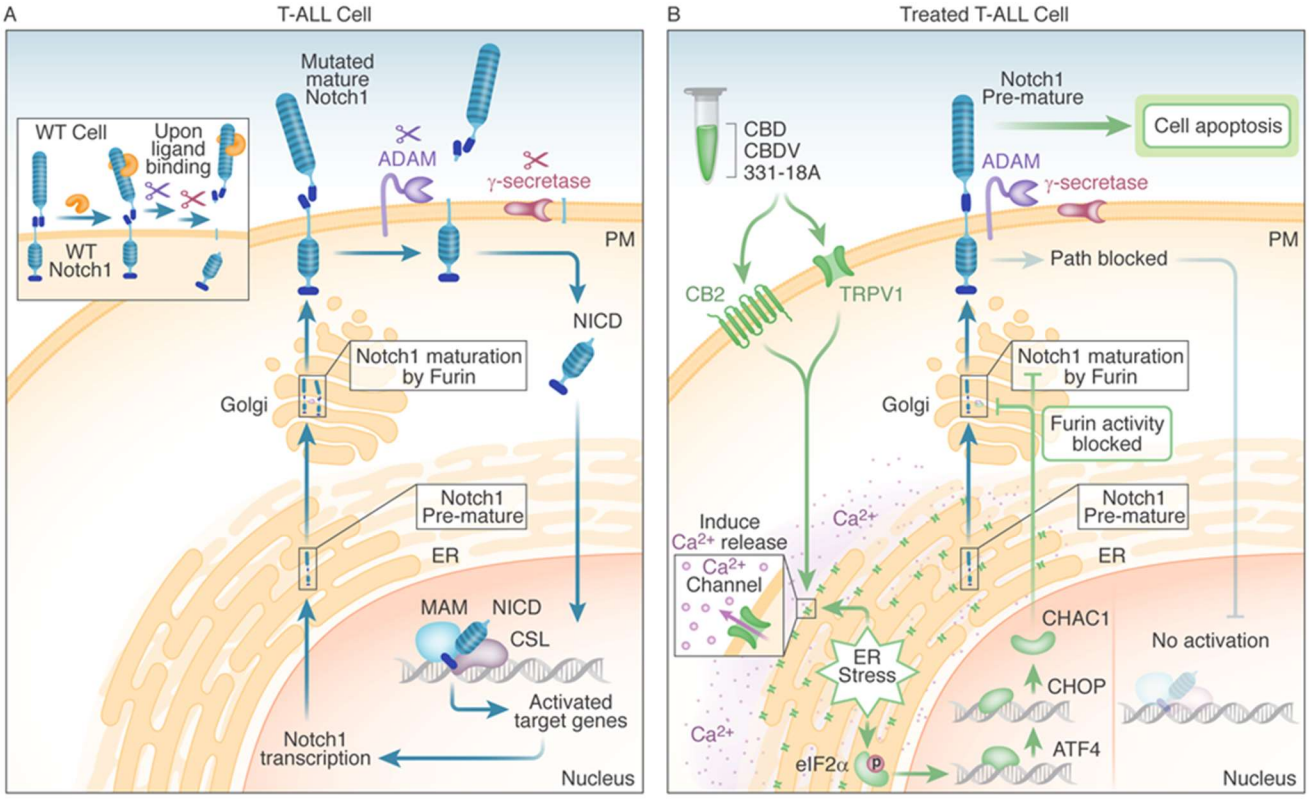


**Fig. 7. Schematic representation.** (**A**) In WT cells, the Notch1 receptor is only activated upon ligand binding. In T-ALL cells that have a Notch1 mutation, the receptor is constitutively active regardless of ligand binding, leading to a positive feedback loop in which the mature receptor is cleaved by a series of

328 sequential cleavage events, causing the release of NICD, which translocates to the nucleus where it
329 promotes transcription of target genes involved in cell growth. The premature Notch1 is cleaved by a
330 furin-like convertase in the trans-Golgi apparatus, resulting in a mature receptor that is transported to the
331 membrane. (**B**) The three phytocannabinoids CBD, CBDV and 331-18A in the whole extract stimulate
332 CB2 and TRPV1 leading to an increase in cytosolic $Ca^{2+}$ and ER stress induced activation of eIF2α
333 followed by ATF4-CHOP-CHAC1 signaling. CHAC1 inhibits the furin-like cleavage of Notch1,
334 preventing its maturation and resulting in reduced NICD formation, reduced cell viability and increased
335 apoptosis.

336 **Materials and Methods**

337 **Reagents.** The analytical standards (>98%) for phytocannabinoids were purchased from Silicol Scientific
338 Equipment Ltd. (Or Yehuda, Israel). The antagonists CID 16020046 (#4959/5), AM630 (#1120/10), SR-
339 144,528 (#5039/10) and AMG9810 (#2316/10) were purchased from Tocris Bioscience (Bristol, UK).
340 BIM-46187 (#5332990001) and ISRIB (#SML0843) were purchased from Sigma-Aldrich (Rehovot,
341 Israel). Synthetic CBD, CBDV and 331-18A ware purchased from Cannasoul Analytics (Caesarea, Israel).
342 **Phytocannabinoids analysis.** Comprehensive phytocannabinoid analysis was performed using a UHPLC
343 system coupled to a Q Exactive™ Focus Hybrid Quadrupole-Orbitrap MS (Thermo Scientific, Bremen,
344 Germany) using a similar chromatographic method as previously described (*29*, *32*). MS acquisition was
345 carried out with a heated electro spray ionization (HESI-II) ion source operated in negative mode. Source
346 parameters were as follows: sheath gas flow rate, auxiliary gas flow rate and sweep gas flow rate: 50, 20
347 and 0 arbitrary units respectively; capillary temperature: 350°C; heater temperature: 50°C; spray voltage:
348 3.00 kV. The scan range was 150–550 m/z for all acquisition events. MS was operated in full $MS^1$ mode
349 at 70,000 resolution, and the AGC target was set to $10^6$ with a maximum IT of 100 ms. Identification and
350 absolute quantification of phytocannabinoids was performed by external calibrations as described by
351 Berman *et al*.(*29*). Absolute quantification of phytocannabinoids with analytical standards was performed
352 by external calibrations. Standard mixes were prepared ranging from 1 to 1000 ng/mL for $\Delta^9$-THCA, $\Delta^9$-
353 THC, CBDA and CBD, and 0.25 to 625 ng/mL for all the other components. The dynamic range for each
354 component was determined as maximum deviation from expected concentrations of 20%, and minimum
355 signal-to-noise ratios of 10. All other phytocannabinoids without analytical standards were semi-
356 quantified according to calibration curves from the same phytocannabinoid family or average curves for
357 unknown compounds (*29*). All samples were injected and analyzed by ESI-LC/MS in three concentrations
358 (10, 1 and 0.1 µg/mL Cannabis extract to ethanol).

359 **Isolation of single phytocannabinoids.** Fractionation of the whole Cannabis extract into four fractions
360 and isolation of single phytocannabinoids were performed using a semi-preparative HPLC/UV (Thermo
361 Scientific, Bremen, Germany). The chromatographic separation was achieved using a Luna® C18 column
362 (10 µm, 250 mm × 21.1 mm i.d.) and a two-solvent A/B multistep gradient (solvent A: 0.1% acetic acid
363 in water and solvent B: 0.1% acetic acid in acetonitrile, the solvents and acetic acid were of HPLC and
364 LC/MS grades, respectively). The multistep gradient program was established as follows: initial
365 conditions were 50% B for 4 min, raised to 76% B until 6.5 min, held at 76% B for 16.5 min, and then
366 raised to 90% B until 26 min, held at 90% B until 31 min, decreased to 50% B over the next 4 min, and
367 held at 50% B until 40 min for re-equilibration of the system prior to the next injection. A flow rate of 20
368 ml/min and an injection volume of 500-750 µl were used. Data acquisition was performed at 220 nm. The
369 crude Cannabis extract was prepared in a concentration of 100 mg/ml in ethanol. Fractions were collected
370 in 10 min intervals and then lyophilized to dryness and analyzed by UHPLC/UV and ESI-LC/MS.
371 To improve the yield and purity of the fractions for isolation of single phytocannabinoids, a preliminary
372 separation step was employed prior to semi-preparative HPLC fractionation. The crude Cannabis extract
373 was dissolved to a concentration of 0.5 g/ml in ethanol, filtered using a PTFE 0.45 µm filter, and then
374 purified using a PLC 2050 Purification System, equipped with a CPC-250 column and a photodiode array
375 (PDA) detector (Gilson Inc.). Separations were achieved using a biphasic solvent system consisting of
376 upper (hexane:acetonitrile in the ratio of 98:2 v/v) and mobile (acetonitrile:water in the ratio 50:50 v/v)
377 phases in descending mode. The column was operated with a flow rate of 12.5 ml/min and a rotation speed
378 of 2,200 rpm. The gradient program was established as follows: initial conditions were
379 acetonitrile:water:hexane in the ratio 50:50:0 v/v for 25 min, and then gradually raised to
380 acetonitrile:water:hexane in the ratio 64:34:2 v/v until 45 min. All the solvents were of HPLC grade. The

381 collected fractions were lyophilized to dryness and then subjected to semi-preparative HPLC fractionation.
382 The specific phytocannabinoids were collected according to retention time.

383 **Structure elucidation.** The structure of the isolated 331-18A was elucidated by $^{1}H$ and $^{13}C$ one-
384 dimensional NMR spectra (Avance-III-700, Bruker, Germany) with CBD as the reference. The samples
385 were dissolved in $CDCl_3$ and analyzed at 4ºC with Tetramethylsilane as the internal reference. The optical
386 rotation of 331-18A in comparison to CBD was determined in chloroform (10 mg/mL) using a Jasco P-
387 1010 (Rudolph Research Analytical, US) polarimeter at 26ºC.

388 **Cell culture.** The T-cell leukemia cell lines MOLT-4 (CVCL_0013, CRL-1582™) and CCRF-CEM
389 (CVCL_0207, CCL-119™) were purchased from ATCC. Cell lines were grown in RPMI 1640 media
390 (Sigma-Aldrich; R8758), and kept at 37ºC in a 5% carbon dioxide incubator. Unless otherwise stated, all
391 culture media were supplemented with 10% FBS (Biological Industries; 04-007-1A), penicillin (100
392 U/mL) and streptomycin (100 µg/mL) (Biological Industries; 03-031-1B).

393 **Cell apoptosis assay.** Cells were cultured in 12-well plates at $1\times10^{6}$ cells/well with media containing
394 0.5% FBS and incubated for 24 h with either DMSO (vehicle), Cannabis extract 12, fractions 1-4 and
395 different combinations of 0.06 µg/ml 331-18A, 0.06 µg/ml CBDV and 1.5 µg/ml CBD. Apoptotic cells
396 were detected by an Annexin V/PI assay using flow cytometry or by detection of cleaved caspase-3.

397 **Annexin V/PI assay.** Apoptosis was assessed by Annexin V-FITC (BioVision; 1006-200, 1:500) and PI
398 staining in an annexin binding buffer (BioVision; 1006-100; 1:500) according to the manufacturer's
399 instructions. Apoptosis assessed by flow cytometry used a BD™ LSR II digital four-laser flow cytometer
400 (BD Biosciences) and was analyzed by BD FACSDiva™ software version 6.1.2. (BD Biosciences).
401 Results were calculated as percentage of positive Annexin V-FITC cells out of total cells counted (30,000
402 events).

403 **Western blot analysis.** Cells were quickly washed twice with ice-cold PBS, and lysed in
404 radioimmunoprecipitation assay buffer (RIPA) lysis buffer (Sigma Aldrich; R0278) freshly supplemented
405 with protease and phosphate inhibitors (Cell Signaling Technology; 5872). Lysates were cleared by
406 centrifugation at 13,000 g at 4ºC for 10 min. Protein concentration was determined by a Bradford assay
407 (Sigma Aldrich; B6916). Proteins were denatured in NuPAGE™ LDS Sample Buffer (4X) (Thermo
408 Fisher; NP0008) and supplemented with β-mercaptoethanol (Sigma Aldrich; B6131). Typically, 20-50
409 mg of total protein were loaded per lane on a Novex™ 4-20% Tris-Glycine gradient gel (Invitrogen;
410 XP04202BOX) and electrophoretically transferred to a nitrocellulose membrane (Bio-Rad; 1704159S).
411 Membranes were blocked with TBS 0.1% Tween 20 buffer containing 5% bovine serum albumin (Sigma;
412 A7906) for 1 h and incubated with the primary antibody overnight at 4°C. This was followed by incubation
413 with horseradish peroxidase-labeled matching secondary antibodies. Immunoreactive bands were detected
414 by Luminata™ HRP substrate (Millipore; WBLUR0500) and visualized using a MicroChemi imager
415 (DNR Bioimaging Systems). Antibodies used: Cleaved Notch1 Val1744 (CST, 4147S; AB_2153348;
416 1:1,000) to assess NICD, cleaved caspase-3 (CST, 9664; AB_2070042; 1:1,000), β-tubulin (CST; clone
417 D3U1W, 86298; AB_2715541; 1:1,000), GAPDH (CST, 2118; AB_561053; 1:5,000), ATF4
418 (Proteintech, 10835-1-AP; AB_2058600; 1:500), CHOP (Proteintech, 15204-1-AP; AB_2292610; 1:500),
419 CHAC1 (abcam, ab76386; AB_1658635; 1:500), eIF2α (CST, 5324; AB_10692650; 1:1000) and
420 Phospho-eIF2α (Ser51) (CST, 3398; AB_2096481; 1:1000). Secondary antibodies include: Peroxidase
421 AffiniPure Goat Anti-Rabbit IgG (H+L) (Jackson ImmunoResearch, 111-035-144; AB_2307391;
422 1:5,000) and Peroxidase-AffiniPure Goat anti mouse IgG (HZ+L) (Jackson ImmunoResearch, 115-035-
423 003; AB_10015289; 1:5000).
424 **RNA extraction.** Total RNA was isolated from MOLT-4 cells ($1\times10^6$ cells/sample) using TRIzol®
425 (Thermo Fisher; 15596026) and RNeasy kit (Qiagen; 74104) according to the manufacturer's instructions.

426 Sample quality was assessed both spectrophotometrically (Nanodrop Technologies®) and by gel
427 electrophoresis with 1% agarose.

428 **RNA-seq.** RNA sequencing of differentially expressed genes was performed on extracted RNA with an
429 Affymetrix Clariom-S microarray for human genome RNA expression analysis and an Affymetrix
430 Transcriptome Analysis Console software. The threshold set for increased- and decreased-abundance
431 genes was a fold change ≥1.5 and $p<0.05$. The sequencing was performed by the Center
432 for Genomic Technologies of The Hebrew University of Jerusalem.

433 **Quantitative RT-PCR.** cDNA was synthesized from 1 µg of extracted RNA. Purified RNA was reverse
434 transcribed with the qScript™ cDNA synthesis kit (Quanta Biosciences; 95047). The mRNA expression
435 levels of were quantified using qRT-PCR 7300 system (Applied Biosystems) using Human Taqman
436 probes (Thermo Fisher Scientific) for: *GAPDH* (Hs02758991_g1); *CNR1* (CB1) (Hs01038522_s1); *CNR2*
437 (CB2) (Hs00361490_m1); *GPR55* (Hs00271662_s1); *TRPV1* (Hs00175798_m1); *TRPM8*
438 (Hs01066596_m1); *TRPA1* (Hs00175798_m1); *ATF4* (Hs00909569_g1); *DDIT3* (CHOP)
439 (Hs00358796_g1); *CHAC1* (Hs00225520_m1). Relative expression values were normalized using to the
440 endogenous housekeeping gene *GAPDH* as the control and calculated using standard ΔCT methods.

441 **Calcium imaging.** MOLT-4 Cells were loaded with the fluorescein $Ca^{2+}$ probe Fluo-4 AM (Invitrogen #
442 F14217). Cells were incubated for 60 min in RPMI medium and supplemented with 1 µM Fluo-4/AM.
443 Cells were then rinsed twice and incubated for another 30 min in a Fluo-4 AM-free HBSS buffer (Sigma
444 Aldrich #H6648). During these steps the cells were kept in the dark. Fluo-4 signals were collected by a
445 BD™ LSR II digital four-laser flow cytometer (BD Biosciences) and analyzed by BD FACSDiva™
446 software version 6.1.2. (BD Biosciences).

447 **Cell viability assay.** Cells were cultured in 96-well plates. At $1\times10^5$ cells/well the media was replaced
448 with RPMI containing 0.5% FBS and treatments as indicated. DMSO was used as the vehicle. The XTT-

449 based cell proliferation kit (Sartorius, Beit Haemek, Israel) was used to quantitate viability according to
450 the manufacturer's instructions. Cytotoxicity was measured following 24 hrs of incubation using
451 fluorescence spectrophotometry at excitation and emission wavelengths of 450-500 and 630-690 nm,
452 respectively, and calculated as percent reduction between treated and control cells.

453 **Synergy Scoring**. The cell viability percentage for each concentration was assessed with an XTT-based
454 cell proliferation kit (Sartorius, Beit Haemek, Israel), then entered into SynergyFinder web application (v
455 2.0). The HSA model was used to calculate synergy scores of the cannabinoid combinations. Estimation
456 of outlier measurements was carried out with cNMF algorithm (*66*) implemented in SynergyFinder.

457 **Mice and procedures.** All procedures were performed according to protocols approved by the Technion
458 Administrative Panel of Laboratory Animal Care (animal protocol number: IL_0470317). Female
459 NOD.CB17-Prkdcscid/NCrHsd (IMSR_ENV:HSD-170) adult (6-7 weeks) mice were purchased from
460 Envigo. Female NSG adult (6-7 weeks) mice were purchased from the Technion animal facility.

461 For the in-vivo tumorigenicity assay, MOLT-4 cells mixed with BD Matrigel$^{TM}$ Matrix Growth Factor
462 Reduced (BD; FAL356230) (1:1 v/v) were injected subcutaneously into the flanks of 7-week-old female
463 NOD-scid mice. Tumor size was measured with a caliper, and the tumor volume was determined
464 according to the formula: length x width$^2$ x 0.5. The mice were euthanized after the indicated days as none
465 reached the maximal endpoint size (1 cm$^3$). The xenograft tumors were dissected and weighed.

466 For the in-vivo leukemogenesis assay and survival analysis, CCRF-CEM cells were intravenously injected
467 to 7-week female NSG mice. The bone marrow was harvested from each mouse and the infiltrated CCRF
468 cells were identified by staining for a human CD45 antibody (Biolegend; AB_2687375; BLG-368522;
469 1:200).

470 For the Patient-Derived Xenograft (PDX) model, frozen aliquots of T-ALL patient samples in which
471 Notch1 mutation was verified by next-generation sequencing were purchased from Dana-Farber Cancer

472 Institute. The cells were expanded in mice and injected subcutaneously into the flanks of 7-week female
473 NSG mice. To investigate the inhibitory effects of extract 12 on leukemogenesis, 30 mg/kg/day extract
474 was intraperitoneally injected three times a week, starting three weeks after cell injection. The mice were
475 euthanized after the indicated days. BM, peripheral blood and spleens were harvested from each mouse
476 and the infiltrated primary cells were identified using flow cytometry by staining for human CD45
477 antibody (BioLegend; BLG-368522; 1:200).

478 **Cannabinoids analysis from tumor tissue.** Fresh excised tumors were accurately weighed and dissected
479 to smaller sections. Hanks' Balanced Salt Solution (Sigma Aldrich; H8264) was added in a ratio of 1 ml
480 per 100 mg sample. The samples were further homogenized into single-cell suspensions with a
481 gentleMACS™ Dissociator (Miltenyi Biotec) using a pre-set program for tumor tissues. The single cell
482 suspensions were stored at -80ºC until further extraction. CBD, CBDV and 331-18A were analyzed using
483 the ESI-LC/MS system by retention time, accurate mass and spectral matching against our developed ESI-
484 LC/MS/MS library of phytocannabinoids (*29*). Absolute quantification of the three compounds was
485 performed by the stable isotope dilution method as recently described by our group (*40*). Briefly, the
486 extraction solution (methanol:acetonitrile:acetic acid in the ratio 50:50:0.1 v/v) spiked with 20 ng/mL of
487 CBD-d3 internal standard (Sigma-Aldrich; C-084) was added to the single cell suspensions in the ratio
488 3:1 v/v, respectively. Samples were thoroughly vortexed and then centrifuged for 20 min at 4ºC for protein
489 and cell precipitation. The supernatants were then mixed in a ratio of 1:3 v/v sample to 0.1% v/v acetic
490 acid in water, and loaded onto Agela Cleanert C8 solid phase extraction cartridges (500 mg of sorbent, 50
491 µm particle size). Cannabinoids were eluted from the columns using 2 ml of 0.1% v/v acetic acid in
492 methanol, evaporated to dryness by speedvac, and reconstituted in 100 µl ethanol. Since there was no
493 analytical standard available for 331-18A, this compound was semi-quantified according to the calibration
494 curve of CBD.

495 **Statistics and reproducibility**. Data were analyzed with GraphPad Prism software version 7.04.
496 Statistical significance was determined by either an unpaired two-tailed Student's *t*-test (with unequal
497 variations if an F test ruled out the equal variation assumption) or one-way ANOVA followed by Sidak's
498 multiple comparisons test for multiple groups. Kaplan–Meier survival curves were analyzed with the
499 Gehan–Breslow–Wilcoxon test, as appropriate for the dataset. Data are generally expressed as mean ±
500 SEM, as denoted in the Figure captions, with $p \leq 0.05$ was considered statistically significant.

501 **Supplementary Materials**
502
503 **Table S1**. Phytocannabinoid concentrations by UHPLC/LC-MS of fractions relative to the whole
504 extract.
505
506 **Table S2**. Phytocannabinoid concentrations by UHPLC/LC-MS of cannabis fraction 2 peaks.
507
508 **Table S3**. $^{1}$H and $^{13}$C peak assignments and chemical shifts of 331-18A.
509
510 **Table S4.** Ten most increased- and decreased-abundance genes following treatment of MOLT-4 cells
511 with the whole extract according to Affymetrix.
512
513 **Fig. S1**. Fraction 2 is as effective as the whole extract in reducing the viability of MOLT-4 cells.
514
515 **Fig. S2**. Specific identification of phytocannabinoids with anti-cancer properties by spectral matching
516 and peak purity.
517
518 **Fig. S3**. CBD and 331-18A NMR spectra.
519
520 **Fig. S4**. Notch1 downregulation by Extract 12 is mediated through CB2 and TRPV1 followed by ATF4-
521 CHOP-CHAC1 signaling pathway.
522
523 **Fig. S5**. Whole extract treatment activates eIF2α.
524
525 **Fig. S6**. Inhibition of tumor growth *in-vivo* by whole extract.
526
527 **Fig. S7.** Treatment with extract containing the three cannabinoids inhibits leukemic expansion in an *in-*
528 *vivo* PDX model.

529 **References**
530


531 1. T. Girardi, C. Vicente, J. Cools, K. De Keersmaecker, The genetics and molecular biology of T-
532 ALL. **129**, 1113–1123 (2017).
533 2. E. Vadillo, E. Dorantes-Acosta, R. Pelayo, M. Schnoor, T cell acute lymphoblastic leukemia (T-
534 ALL): New insights into the cellular origins and infiltration mechanisms common and unique
535 among hematologic malignancies. *Blood Rev.* **32**, 36–51 (2018).
536 3. C. Sorrentino, A. Cuneo, G. Roti, Therapeutic Targeting of Notch Signaling Pathway in
537 Hematological Malignancies. *Mediterr. J. Hematol. Infect. Dis.* **11**, e2019037 (2019).
538 4. A. A. Ferrando, The role of NOTCH1 signaling in T-ALL. *Hematol. Am. Soc. Hematol. Educ.*
539 *Progr.*, 353–361 (2009).
540 5. A. C. McCarter, Q. Wang, M. Chiang, Notch in Leukemia. *Adv. Exp. Med. Biol.* **1066**, 355–394
541 (2018).
542 6. Z. Fang-Fang, Y. You, L. Wen-Jun, Progress in research on childhood T-cell acute lymphocytic
543 leukemia, Notch1 signaling pathway, and its inhibitors: A review. *Bosn. J. Basic Med. Sci.*, doi:
544 10.17305/bjbms.2020.4687 (2020).
545 7. M. Katoh, M. Katoh, Precision medicine for human cancers with Notch signaling dysregulation
546 (Review). Spandidos Publications (2020). https://doi.org/10.3892/ijmm.2019.4418.
547 8. H. Qiu, P. M. Zmina, A. Y. Huang, D. Askew, B. Bedogni, Inhibiting Notch1 enhances
548 immunotherapy efficacy in melanoma by preventing Notch1 dependent immune suppressive
549 properties. *Cancer Lett.* **434**, 144–151 (2018).
550 9. M. A. Rice, E. C. Hsu, M. Aslan, A. Ghoochani, A. Su, T. Stoyanova, Loss of Notch1 activity
551 inhibits prostate cancer growth and metastasis and sensitizes prostate cancer cells to antiandrogen
552 therapies. *Mol. Cancer Ther.* **18**, 1230–1242 (2019).
553 10. J. Li, Q. Li, L. Lin, R. Wang, L. Chen, W. Du, C. Jiang, R. Li, Targeting the Notch1 oncogene by
554 miR-139-5p inhibits glioma metastasis and epithelial-mesenchymal transition (EMT). *BMC*
555 *Neurol.* **18**, 133 (2018).
556 11. S. A. Kahn, X. Wang, R. T. Nitta, S. Gholamin, J. Theruvath, G. Hutter, T. D. Azad, L. Wadi, S.
557 Bolin, V. Ramaswamy, R. Esparza, K.-W. Liu, M. Edwards, F. J. Swartling, D. Sahoo, G. Li, R.
558 J. Wechsler-Reya, J. Reimand, Y.-J. Cho, M. D. Taylor, I. L. Weissman, S. S. Mitra, S. H.
559 Cheshier, Notch1 regulates the initiation of metastasis and self-renewal of Group 3
560 medulloblastoma. *Nat. Commun.* **9**, 4121 (2018).
561 12. K. E. Vinson, D. C. George, A. W. Fender, F. E. Bertrand, G. Sigounas, The Notch pathway in
562 colorectal cancer. *Int. J. Cancer* **138**, 1835–1842 (2016).
563 13. F. Punzo, I. Manzo, C. Tortora, E. Pota, V. D'Angelo, G. Bellini, A. Di Paola, F. Verace, F.
564 Casale, F. Rossi, Effects of CB2 and TRPV1 receptors' stimulation in pediatric acute T-
565 lymphoblastic leukemia. *Oncotarget* **9**, 21244–21258 (2018).
566 14. K.-H. Jeon, S.-H. Park, W. J. Bae, S. W. Kim, H. J. Park, S. Kim, T. H. Kim, S. H. Jeon, I. Park,
567 H.-J. Park, Y. Kwon, Cannabidiol, a Regulator of Intracellular Calcium and Calpain. *Cannabis*
568 *cannabinoid Res.*, doi: 10.1089/CAN.2021.0197 (2022).
569 15. C. Muller, P. Morales, P. H. Reggio, E. Murillo-Rodriguez, C. Chiu, J. Hee Hong, Cannabinoid
570 Ligands Targeting TRP Channels. doi: 10.3389/fnmol.2018.00487 (2019).
571 16. A. Laguerre, K. Keutler, S. Hauke, C. Schultz, Regulation of Calcium Oscillations in β-Cells by
572 Co-activated Cannabinoid Receptors. *Cell Chem. Biol.* **28**, 88-96.e3 (2021).
573 17. D. I. Abrams, M. Guzman, Cannabis in cancer care. *Clin. Pharmacol. Ther.* **97**, 575–586 (2015).
574 18. D. I. Abrams, Using Medical Cannabis in an Oncology Practice. *Oncology* **30**, 397–404 (2016).

575 19. M. Duran, E. Pérez, S. Abanades, X. Vidal, C. Saura, M. Majem, E. Arriola, M. Rabanal, A.
576 Pastor, M. Farré, N. Rams, J.-R. R. Laporte, D. Capellà, Preliminary efficacy and safety of an
577 oromucosal standardized cannabis extract in chemotherapy-induced nausea and vomiting. *Br. J.*
578 *Clin. Pharmacol.* **70**, 656–663 (2010).
579 20. C. Pagano, G. Navarra, L. Coppola, M. Bifulco, C. Laezza, Molecular Mechanism of
580 Cannabinoids in Cancer Progression. *Int. J. Mol. Sci.* **22**, 3680 (2021).
581 21. O. Kovalchuk, I. Kovalchuk, Cannabinoids as anticancer therapeutic agents. *Cell Cycle* **19**, 961–
582 989 (2020).
583 22. E. M. O'Reilly, J. M. Cosgrave, W. M. Gallagher, A. S. Perry, Plant-derived cannabinoids as
584 anticancer agents. *Trends in cancer* **8**, 350–357 (2022).
585 23. C. Blázquez, L. González-Feria, L. Álvarez, A. Haro, M. L. Casanova, M. Guzmán, Cannabinoids
586 inhibit the vascular endothelial growth factor pathway in gliomas. *Cancer Res.* **64**, 5617–5623
587 (2004).
588 24. S. D. McAllister, L. Soroceanu, P.-Y. Y. Desprez, The Antitumor Activity of Plant-Derived Non-
589 Psychoactive Cannabinoids. *J. Neuroimmune Pharmacol.* **10**, 255–267 (2015).
590 25. B. Hinz, R. Ramer, Cannabinoids as anticancer drugs: current status of preclinical research. *Br. J.*
591 *Cancer 2022 1271* **127**, 1–13 (2022).
592 26. K. M. Kampa-Schittenhelm, O. Salitzky, F. Akmut, B. Illing, L. Kanz, H. R. Salih, M. M.
593 Schittenhelm, Dronabinol has preferential antileukemic activity in acute lymphoblastic and
594 myeloid leukemia with lymphoid differentiation patterns. *BMC Cancer* **16**, 25 (2016).
595 27. K. A. Scott, A. G. Dalgleish, W. M. Liu, Anticancer effects of phytocannabinoids used with
596 chemotherapy in leukaemia cells can be improved by altering the sequence of their
597 administration. *Int. J. Oncol.* **51**, 369–377 (2017).
598 28. M. Olivas-Aguirre, L. Torres-López, J. S. Valle-Reyes, A. Hernández-Cruz, I. Pottosin, O.
599 Dobrovinskaya, Cannabidiol directly targets mitochondria and disturbs calcium homeostasis in
600 acute lymphoblastic leukemia. *Cell Death Dis.* **10**, 779 (2019).
601 29. P. Berman, K. Futoran, G. M. Lewitus, D. Mukha, M. Benami, T. Shlomi, D. Meiri, A new ESI-
602 LC/MS approach for comprehensive metabolic profiling of phytocannabinoids in Cannabis. *Sci.*
603 *Rep.* **8**, 14280 (2018).
604 30. L. O. Hanuš, S. M. Meyer, E. Muñoz, O. Taglialatela-Scafati, G. Appendino, Phytocannabinoids:
605 a unified critical inventory. *Nat. Prod. Rep.* **33**, 1357–1392 (2016).
606 31. L. Baram, E. Peled, P. Berman, B. Yellin, E. Besser, M. Benami, I. Louria-Hayon, G. M.
607 Lewitus, D. Meiri, The heterogeneity and complexity of *Cannabis* extracts as antitumor agents.
608 *Oncotarget* **10**, 4091–4106 (2019).
609 32. E. Besser, A. Gelfand, G. M. Lewitus, H. Novak-Kotzer, S. Procaccia, P. Berman, I. Louria-
610 Hayon, I. Shreiber-Livne, Y. Ofran, D. Meiri, Antitumoral effects of cannabis in Notch1-mutated
611 T-cell acute lymphoblastic leukemia. *Cancer Commun.* **43**, 711–715 (2023).
612 33. L. Marchetti, V. Brighenti, M. C. Rossi, J. Sperlea, F. Pellati, D. Bertelli, Use of 13C-qNMR
613 Spectroscopy for the Analysis of Non-Psychoactive Cannabinoids in Fibre-Type Cannabis sativa
614 L. (Hemp). *Molecules* **24** (2019).
615 34. P.-H. Chen, W.-L. Shen, C.-M. Shih, K.-H. Ho, C.-H. Cheng, C.-W. Lin, C.-C. Lee, A.-J. Liu, K.-
616 C. Chen, The CHAC1-inhibited Notch3 pathway is involved in temozolomide-induced glioma
617 cytotoxicity. *Neuropharmacology* **116**, 300–314 (2017).
618 35. Z. Chi, J. Zhang, A. Tokunaga, M. M. Harraz, S. T. Byrne, A. Dolinko, J. Xu, S. Blackshaw, N.
619 Gaiano, T. M. Dawson, V. L. Dawson, Botch promotes neurogenesis by antagonizing Notch. *Dev.*
620 *Cell* **22**, 707–20 (2012).

621 36. J. H. Joo, E. Ueda, C. D. Bortner, X. P. Yang, G. Liao, A. M. Jetten, Farnesol activates the
622 intrinsic pathway of apoptosis and the ATF4-ATF3-CHOP cascade of ER stress in human T
623 lymphoblastic leukemia Molt4 cells. *Biochem. Pharmacol.* **97**, 256–268 (2015).
624 37. K. Zhai, A. Liskova, P. Kubatka, D. Büsselberg, Calcium entry through trpv1: A potential target
625 for the regulation of proliferation and apoptosis in cancerous and healthy cells. *Int. J. Mol. Sci.*
626 **21**, 1–25 (2020).
627 38. M. Halliday, G. R. Mallucci, Review: Modulating the unfolded protein response to prevent
628 neurodegeneration and enhance memory. *Neuropathol. Appl. Neurobiol.* **41**, 414–427 (2015).
629 39. B. Yadav, K. Wennerberg, T. Aittokallio, J. Tang, Searching for Drug Synergy in Complex
630 Dose–Response Landscapes Using an Interaction Potency Model. *Comput. Struct. Biotechnol. J.*
631 **13**, 504–513 (2015).
632 40. P. Berman, L. Sulimani, A. Gelfand, K. Amsalem, G. M. Lewitus, D. Meiri, Cannabinoidomics –
633 An analytical approach to understand the effect of medical Cannabis treatment on the
634 endocannabinoid metabolome. *Talanta*, 121336 (2020).
635 41. M. W. Lee, H. J. Kim, K. H. Yoo, D. S. Kim, J. M. Yang, H. R. Kim, Y. H. Noh, H. Baek, H.
636 Kwon, M. H. Son, S. H. Lee, H. W. Cheuh, H. L. Jung, K. W. Sung, H. H. Koo, Establishment of
637 a bioluminescent imaging-based in vivo leukemia model by intra-bone marrow injection. *Int. J.*
638 *Oncol.* **41**, 2047–2056 (2012).
639 42. Q. Xin, Z. Chen, W. Wei, Y. Wu, Animal models of acute lymphoblastic leukemia:
640 Recapitulating the human disease to evaluate drug efficacy and discover therapeutic targets.
641 *Biochem. Pharmacol.* **198**, 114970 (2022).
642 43. R. A. Previs, R. L. Coleman, A. L. Harris, A. K. Sood, Molecular pathways: Translational and
643 therapeutic implications of the notch signaling pathway in cancer. *Clin. Cancer Res.* **21**, 955–961
644 (2015).
645 44. E. B. Russo, J. Marcu, Cannabis Pharmacology: The Usual Suspects and a Few Promising Leads.
646 *Adv. Pharmacol.* **80**, 67–134 (2017).
647 45. G. Velasco, C. Sánchez, M. Guzmán, Anticancer mechanisms of cannabinoids. *Curr. Oncol.* **23**,
648 S23-32 (2016).
649 46. M. Guzmán, Cannabinoids: Potential anticancer agents. *Nat. Rev. Cancer* **3**, 745–755 (2003).
650 47. P. Stoss, P. Merrath, A Useful Approach Towards Δ9 -Tetrahydrocannabinol. *Synlett* **1991**, 553–
651 554 (1991).
652 48. E. B. Russo, Taming THC: Potential cannabis synergy and phytocannabinoid-terpenoid entourage
653 effects. *Br. J. Pharmacol.* **163**, 1344–1364 (2011).
654 49. T. Worth, Cannabis's chemical synergies. *Nature* **572**, S12–S13 (2019).
655 50. S. Blasco-Benito, M. Seijo-Vila, M. Caro-Villalobos, I. Tundidor, C. Andradas, E. García-
656 Taboada, J. Wade, S. Smith, M. Guzmán, E. Pérez-Gómez, M. Gordon, C. Sánchez, Appraising
657 the "entourage effect": Antitumor action of a pure cannabinoid versus a botanical drug
658 preparation in preclinical models of breast cancer. *Biochem. Pharmacol.* **157**, 285–293 (2018).
659 51. S. Ben-Shabat, E. Fride, T. Sheskin, T. Tamiri, M.-H. H. Rhee, Z. Vogel, T. Bisogno, L. De
660 Petrocellis, V. Di Marzo, R. Mechoulam, An entourage effect: inactive endogenous fatty acid
661 glycerol esters enhance 2-arachidonoyl-glycerol cannabinoid activity. *Eur. J. Pharmacol.* **353**,
662 23–31 (1998).
663 52. R. Mechoulam, S. Ben-Shabat, From gan-zi-gun-nu to anandamide and 2-arachidonoylglycerol:
664 The ongoing story of cannabis. *Nat. Prod. Rep.* **16**, 131–143 (1999).
665 53. E. B. Russo, The Case for the Entourage Effect and Conventional Breeding of Clinical Cannabis:
666 No "Strain", No Gain. *Front. Plant Sci.* **9**, 1969 (2018).

667 54. V. Di Marzo, F. Piscitelli, The Endocannabinoid System and its Modulation by
668 Phytocannabinoids. *Neurotherapeutics* **12**, 692–698 (2015).
669 55. B. Kis, F. C. Ifrim, V. Buda, S. Avram, I. Z. Pavel, D. Antal, V. Paunescu, C. A. Dehelean, F.
670 Ardelean, Z. Diaconeasa, C. Soica, C. Danciu, Cannabidiol—from Plant to Human Body: A
671 Promising Bioactive Molecule with Multi-Target Effects in Cancer. *Int. J. Mol. Sci.* **20**, 5905
672 (2019).
673 56. L. de Petrocellis, P. Orlando, A. S. Moriello, G. Aviello, C. Stott, A. A. Izzo, V. di Marzo,
674 Cannabinoid actions at TRPV channels: effects on TRPV3 and TRPV4 and their potential
675 relevance to gastrointestinal inflammation. *Acta Physiol.* **204**, 255–266 (2012).
676 57. A. Carracedo, M. Lorente, A. Egia, C. Blázquez, S. García, V. Giroux, C. Malicet, R. Villuendas,
677 M. Gironella, L. González-Feria, M. A. Piris, J. L. Iovanna, M. Guzmán, G. Velasco, The stress-
678 regulated protein p8 mediates cannabinoid-induced apoptosis of tumor cells. *Cancer Cell* **9**, 301–
679 12 (2006).
680 58. K. Ohta, A. Mizuno, S. Li, M. Itoh, M. Ueda, E. Ohta, Y. Hida, M. xing Wang, M. Furoi, Y.
681 Tsuzuki, M. Sobajima, Y. Bohmoto, T. Fukushima, M. Kobori, T. Inuzuka, T. Nakagawa,
682 Endoplasmic reticulum stress enhances γ-secretase activity. *Biochem. Biophys. Res. Commun.*
683 **416**, 362–366 (2011).
684 59. H. Koike, M. Harada, A. Kusamoto, Z. Xu, T. Tanaka, N. Sakaguchi, C. Kunitomi, J. M. K.
685 Azhary, N. Takahashi, Y. Urata, Y. Osuga, Roles of endoplasmic reticulum stress in the
686 pathophysiology of polycystic ovary syndrome. *Front. Endocrinol. (Lausanne).* **14**, 1124405
687 (2023).
688 60. J. Izrailit, A. Jaiswal, W. Zheng, M. F. Moran, M. Reedijk, Cellular stress induces TRB3/USP9x-
689 dependent Notch activation in cancer. *Oncogene 2017 368* **36**, 1048–1057 (2016).
690 61. Y. Ding, X. Chen, B. Wang, B. Yu, J. Ge, Deubiquitinase inhibitor b-AP15 activates endoplasmic
691 reticulum (ER) stress and inhibits Wnt/Notch1 signaling pathway leading to the reduction of cell
692 survival in hepatocellular carcinoma cells. *Eur. J. Pharmacol.* **825**, 10–18 (2018).
693 62. E. Rosati, R. Sabatini, F. De Falco, B. Del Papa, F. Falzetti, M. Di Ianni, L. Cavalli, K.
694 Fettucciari, A. Bartoli, I. Screpanti, P. Marconi, γ-Secretase inhibitor I induces apoptosis in
695 chronic lymphocytic leukemia cells by proteasome inhibition, endoplasmic reticulum stress
696 increase and notch down-regulation. *Int. J. Cancer* **132**, 1940–1953 (2013).
697 63. I. N. Mungrue, J. Pagnon, O. Kohannim, P. S. Gargalovic, A. J. Lusis, CHAC1/MGC4504 Is a
698 Novel Proapoptotic Component of the Unfolded Protein Response, Downstream of the ATF4-
699 ATF3-CHOP Cascade. *J. Immunol.* **182**, 466–476 (2009).
700 64. J. Jung, H. S. Seol, S. Chang, The Generation and Application of Patient-Derived Xenograft
701 Model for Cancer Research. *Cancer Res. Treat.* **50**, 1–10 (2018).
702 65. P. Richter-Pechańska, J. B. Kunz, B. Bornhauser, C. von Knebel Doeberitz, T. Rausch, B.
703 Erarslan-Uysal, Y. Assenov, V. Frismantas, B. Marovca, S. M. Waszak, M. Zimmermann, J.
704 Seemann, M. Happich, M. Stanulla, M. Schrappe, G. Cario, G. Escherich, K. Bakharevich, R.
705 Kirschner-Schwabe, C. Eckert, M. U. Muckenthaler, J. O. Korbel, J. Bourquin, A. E. Kulozik,
706 PDX models recapitulate the genetic and epigenetic landscape of pediatric T-cell leukemia .
707 *EMBO Mol. Med.* **10**, 9443 (2018).
708 66. A. Ianevski, A. K. Giri, P. Gautam, A. Kononov, S. Potdar, J. Saarela, K. Wennerberg, T.
709 Aittokallio, Prediction of drug combination effects with a minimal set of experiments. *Nat. Mach.*
710 *Intell.* **1**, 568–577 (2019).

**Acknowledgments**

We thank the the Israel Cancer Research Fund, Evelyn Gruss Lipper Charitable Foundation and the Israeli Ministry of Agriculture and Rural Development for their financial support of this work. The authors would like to thank Cannasoul Analytics and especially Dr. Rotem Perry Feigenbaum and Yogev Nir for the isolation of the phytocannabinoid compounds; Dr. Hugo Gottlieb and Dr. Michal Afri from the NMR unit at Bar Ilan University for performing the NMR measurements and deciphering the structure of the 331-18A phytocannabinoid; Moshe Barkaly for the semi-preparative HPLC fractionations of the whole extract; and Dr. Dafna Antes for the graphic scheme illustration. The authors declare no competing financial interests.

**Funding:**

Israel Cancer Research Fund grant 21-112-PG (DM)
Gruss Lipper Charitable Foundation grant 2027093 (DM)
Israeli Ministry of Agriculture and Rural Development 14370001 (DM)

**Author contributions:**

Conceptualization: E.B., S.P. and D.M.
Methodology: E.B. and P.B.
Investigation: E.B., A.G. and P.B.
Analysis and interpretation of data: E.B., A.G., P.B and S.P.
Writing-original draft: E.B. and D.M.
Writing-review & editing: E.B., D.M., P.B. and S.P.
Study supervision: D.M.

**Competing interests**

A patent pertaining to the results of the paper has been applied for the use of cannabinoids in the treatment of Notch-related diseases. This patent was licensed to Cavnox Ltd. to test the combination of the molecules in human clinical trials.

**Data and materials availability**

The RNA-Seq data that support the findings of this study have been deposited in the Gene Expression Omnibus under the accession code GSE154287.
https://www.ncbi.nlm.nih.gov/geo/query/acc.cgi?acc=GSE154287.
All data generated or analyzed during this study are included in this published article and its supplementary information files.